

Mask-PINNs: Regulating Feature Distributions in Physics-Informed Neural Networks

Feilong Jiang^a Xiaonan Hou^a Jianqiao Ye^a Min Xia^{b*}

^a Department of Engineering, Lancaster University, LA1 4YW Lancaster, U.K.

^b Department of Mechanical and Materials Engineering, University of Western Ontario, London, Ontario, Canada
min.xia@uwo.ca

Abstract

Physics-Informed Neural Networks (PINNs) are a class of deep learning models designed to solve partial differential equations by incorporating physical laws directly into the loss function. However, the internal covariate shift, which has been largely overlooked, hinders the effective utilization of neural network capacity in PINNs. To this end, we propose Mask-PINNs, a novel architecture designed to address this issue in PINNs. Unlike traditional normalization methods such as BatchNorm or LayerNorm, we introduce a learnable, nonlinear mask function that constrains the feature distributions without violating underlying physics. The experimental results show that the proposed method significantly improves feature distribution stability, accuracy, and robustness across various activation functions and PDE benchmarks. Furthermore, it enables the stable and efficient training of wider networks — a capability that has been largely overlooked in PINNs.

1 Introduction

Partial Differential Equations (PDEs) are widely used in physics, engineering, and finance to model changes in physical quantities with respect to multiple continuous variables, such as time and space. In recent years, Physics-Informed Neural Networks (PINNs) have emerged as a powerful approach for solving PDEs [1]. By incorporating the given PDEs, as well as boundary and initial conditions as loss terms, PINNs ensure that the learned solutions remain consistent with the underlying physics. Leveraging automatic differentiation to compute derivatives, PINNs can approximate the solution without meshing, which allows PINNs to handle irregular geometries and high-dimensional problems more effectively. Additionally, PINNs can seamlessly integrate observed data, making them useful for real-world applications with incomplete information [2-5].

Despite their success, the training process of PINNs still encounters significant difficulties. Since their performance strongly depends on activation functions, some researchers proposed algorithms on automatically learning or adapting these functions to enhance training efficiency and stability [6], [7]. PINNs suffer from initialization pathologies, which causes degradation as the structure goes deeper. New structures as PirateNets, HyResPINNs and Deeper-PINNs are proposed to address this problem [8-10]. Since the training of PINNs involves multiple competing objectives, directional conflicts between different loss terms during training will hinder the convergence of PINNs. Gradient alignment methods have been proposed to facilitate more stable and conflict-free training [11], [12]. Poor initial choices can lead to vanishing or exploding gradients and slow convergence, especially for deeper PINNs structures. Consequently, theoretically informed approaches are proposed to ensure stable training and robust convergence in PINNs [13], [14].

Nevertheless, one critical issue that remains insufficiently addressed is internal covariate shift, which disrupts feature distributions during training and undermines the stability and

expressiveness of PINNs [15]. Traditional normalization techniques, such as BatchNorm and LayerNorm, are typically employed to mitigate these issues in standard deep learning settings. However, these methods depend on global statistics and can disrupt the crucial physics-driven relationships that PINNs rely on. Consequently, the need for an effective yet physics-compatible method of controlling feature distributions of PINNs remains open. To this end, we propose Mask-PINN which fills the gap in alleviating the internal covariate shift of PINNs. The learnable nonlinear mask functions are introduced into PINNs to regulate the feature distributions. We demonstrate Mask-PINNs can enhance training stability and solution accuracy across several benchmarks. Besides, it enables effective use of wider networks, a challenge rarely explored in PINNs.

The remainder of the paper is organized as follows: Section 2 reviews relevant prior work and discusses key limitations; Section 3 introduces Mask-PINNs in detail; Section 4 presents comprehensive experimental validation; and finally, Section 5 summarizes the findings and discusses potential directions for future research.

2 Background

This section introduces the working principle of PINNs. We also briefly discuss traditional normalization techniques' limitations in PINNs.

2.1 Physics-informed Neural Networks

Given the following partial differential equation (PDE):

$$\mathbf{u}_t + \mathcal{N}[\mathbf{u}(t, x)] = 0, \quad t \in [0, T], \quad x \in \Omega, \quad (1)$$

governed by the initial and boundary conditions:

$$\mathbf{u}(0, x) = \mathbf{u}^0(x), \quad x \in \Omega, \quad (2)$$

$$\mathcal{B}[\mathbf{u}] = 0, \quad t \in [0, T], \quad x \in \partial\Omega, \quad (3)$$

where $\mathbf{u}(t, x)$ indicates the solution, $\mathcal{N}[\cdot]$ represents a linear or nonlinear differential operator, $\mathcal{B}[\cdot]$ indicates boundary operator.

The task of PINNs is approximating the solution of the given PDE by a deep neural network (DNN) $\mathbf{u}_\theta(t, x)$, where θ denotes all trainable parameters. For PINNs, $\mathbf{u}_\theta(t, x)$ is constrained by the following loss function:

$$\mathcal{L}(\theta) = \lambda_{ic} \mathcal{L}_{ic}(\theta) + \lambda_{bc} \mathcal{L}_{bc}(\theta) + \lambda_r \mathcal{L}_r(\theta), \quad (4)$$

where

$$\mathcal{L}_{ic}(\theta) = \frac{1}{N_{ic}} \sum_{i=1}^{N_{ic}} \left| \mathbf{u}_\theta(0, x_{ic}^i) - \mathbf{u}^0(x_{ic}^i) \right|^2, \quad (5)$$

$$\mathcal{L}_{bc}(\theta) = \frac{1}{N_{bc}} \sum_{i=1}^{N_{bc}} \left| \mathcal{B}[\mathbf{u}_\theta](t_{bc}^i, x_{bc}^i) \right|^2, \quad (6)$$

$$\mathcal{L}_r(\theta) = \frac{1}{N_r} \sum_{i=1}^{N_r} \left| \frac{\partial \mathbf{u}_\theta}{\partial t}(t_r^i, x_r^i) + \mathcal{N}[\mathbf{u}_\theta](t_r^i, x_r^i) \right|^2, \quad (7)$$

λ is responsible for balancing the weight of different loss terms.

2.2 Feature Distributions of PINNs

It's commonly known that during the training the feature distributions drift away from a centered distribution. For bounded activation functions, the outputs tend to approach their upper or lower limits during training, a phenomenon referred to as the saturation issue [16]. It is known to induce gradient vanishing and reduce the nonlinear capacity as the activation

functions become practically linear in these saturated regions [17-19]. Although the gradient vanishing issue can be alleviated by unbounded activation functions, some commonly used unbounded activation functions still get impaired by the drifting feature distributions. For example, activation functions like GELU, SiLU, and Softplus etc. have regions that behave almost linearly as the inputs locate far from the centre. Such regions limit the nonlinear representational capacity of the network [17], [20]. Consequently, the model struggles to capture complex nonlinear patterns.

Commonly used method for resolving such an issue is the application of normalization techniques [15], [21], [22]. However, the mean subtraction and variance scaling in the normalization like Batch Normalization (BN) or Layer Normalization (LN) can destroy the physical relationships between the inputs and outputs of PINNs. In the following, we demonstrate this issue with experiment on the heat conduction problem:

$$\frac{\partial u}{\partial t} - \frac{\partial^2 u}{\partial x^2} = 0, (x, t) \in [0, 1] \times [0, 1], \quad (8)$$

$$u(x, 0) = \sin(\pi x), x \in [0, 1], \quad (9)$$

$$u(0, t) = u(1, t) = 0, t \in [0, 1], \quad (10)$$

the analytical solution for this problem is:

$$u(x, t) = \sin(\pi x) \cdot \exp(-t\pi^2). \quad (11)$$

All the outcomes are averaged from 5 independent trials. As shown in Fig 1, BN based PINN (BN-PINN), and LN based PINN (LN-PINN) show worse results than Vanilla PINN. For BN-PINN, even though the loss curve decreases during the training, the relative L^2 error curve almost stays flat. This indicates that for PINN with BN, the model is not trained with the given physical constraint. Although LN-PINN obtains consistent decreasing on both and loss relative L^2 error, the accuracy is lower than that of vanilla method. its accuracy remains lower than that of the vanilla method. This indicates that LN hampers the model's ability to capture physical details.

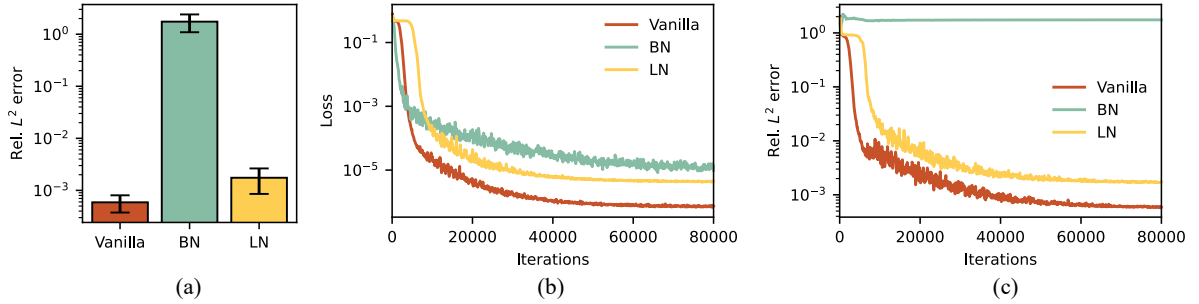


Figure 1. Performance comparison of Vanilla PINN, BN-PINN and LN-PINN. (a) Mean relative L^2 error. (b) Averaged loss curve. (c) Averaged relative L^2 error curve.

3 Methodology

In this section, we introduce the Mask-PINNs, a novel architecture specifically designed to mitigate the internal covariate shift of PINNs. The structure of the proposed method is shown in Fig 2. Each block contains 2 mask layers with shortcut connection to prevent the vanishing or exploding issues.

The mask function can be expressed as:

$$F(\mathbf{x}) = 1 - \exp\left[(-\alpha\mathbf{x})^2\right] \quad (12)$$

where α is a learnable vector scaler that controls the shape of the mask function. Fig. 3 shows the visualization of the proposed mask function. As can be seen, the proposed function shows 0 when the input is 0 and smoothly approach saturation at 1 as the input moves away from 0 in both positive and negative directions.

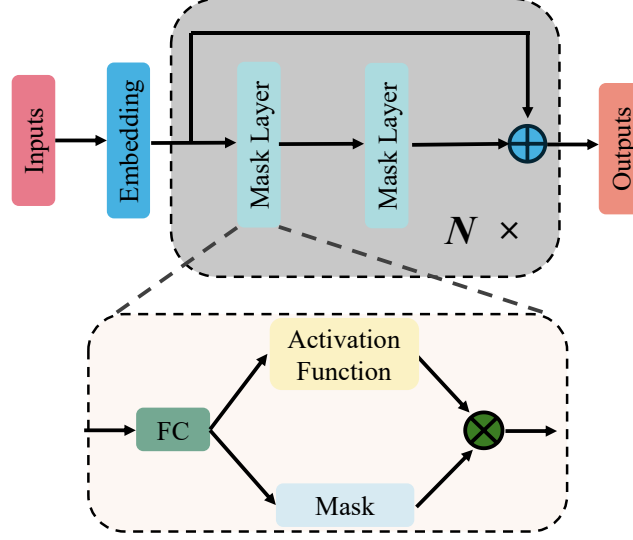


Figure 2. Illustration of the architecture of the Mask-PINNs.

The feed forward process of a block can be expressed as below:

$$z^{(1)} = w^{(1)}H + b^{(1)}, \quad (13)$$

$$H^{(1)} = F^{(1)}(z^{(1)}) \odot \sigma(z^{(1)}), \quad (14)$$

$$\begin{aligned} z^{(2)} &= w^{(2)}H^{(1)} + b^{(2)} \\ &= w^{(2)}[F^{(1)}(z^{(1)}) \odot \sigma(z^{(1)})] + b^{(2)}, \end{aligned} \quad (15)$$

$$H^{(2)} = F^{(2)}(z^{(2)}) \odot \sigma(z^{(2)}), \quad (16)$$

where z represents the pre-activation, H denotes the output of a layer, w represents weights and b represents biases. While $F(z)$ increases with $|z|$, its smooth saturating shape causes the composite output $F(z) \odot \sigma(z)$ to grow more slowly than $\sigma(z)$. As a result, the mask function effectively reduces the occurrence of extreme values and squashes the feature distributions. Besides, the mask function is a transformation that only depends on the neuron's own value without globally normalizing or altering the physical input-output mapping, which is a crucial requirement for PINNs.

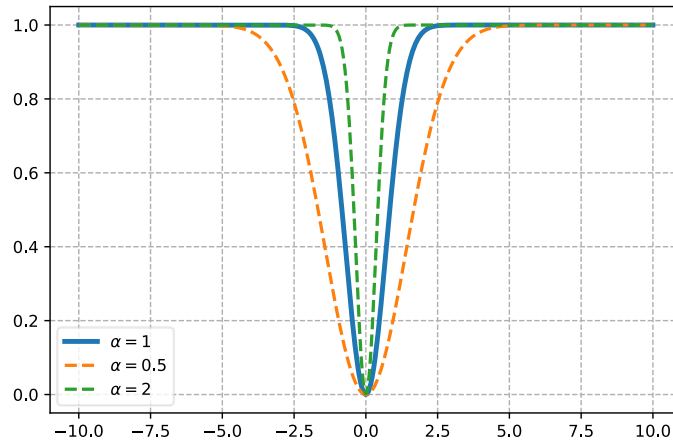


Figure 3. Mask function with different α values. For visualization purposes, we plot the mask function assuming scalar α values, although in practice α is a learnable vector applied independently to each input feature.

4 Experiments

To demonstrate the effectiveness of the proposed method, we conducted experiments across several benchmarks. The methods compared against the proposed methods include Vanilla PINNs, locally adaptive activation functions (LAAF) based PINNs, ResNet based PINNs (ResNet-PINN), PirateNets and ABU-PINN. All the methods are trained with Tanh, GELU, SiLU and SoftPlus as activation functions. Note that ABU-PINN is specifically designed to automatically select activation functions during training, and therefore produces only one result, while the other methods are evaluated separately with each of the four activation functions. Due to the difference of the structure, the depth of each model may vary, but the total trainable parameters are kept about the same number. Adam is utilized as the optimizer. All experiments are conducted on a single NVIDIA GeForce RTX 4090 GPU. All results are averaged over 5 independent trials.

4.1 Convection Equation

We consider convection equation expressed as below:

$$\frac{\partial u}{\partial t} + \beta \frac{\partial u}{\partial x} = 0, x \in [0, 2\pi], t \in [0, 1], \quad (17)$$

$$u(0, x) = \sin(x), \quad (18)$$

$$u(t, 0) = u(t, 2\pi), \quad (19)$$

where we set β as 30.

Each model is composed of 13 hidden layers, each containing 256 neurons, and is trained for 50,000 iterations. For the proposed method, α is initialized with all entries set to 1.0.

Table 1 shows the outcomes of different models. The best-performing method under each activation function is underlined, while the overall best result across all methods is highlighted in bold. As can be seen, the proposed method achieves consistent best results among different activation functions. For Tanh, the proposed method achieves performance an error 1 order of magnitude lower than vanilla method. For SoftPlus, the best result of the proposed method is 2 orders of magnitude lower than vanilla method and almost 1 order smaller than the second-best result.

Table 1: Convection equation: relative L^2 error of different models.

Method	Tanh	GELU	SiLU	SoftPlus
Vanilla	7.29e-3	9.91e-4	1.37e-3	3.55e-1
ResNet-PINN	1.75e-2	1.74e-3	1.50e-3	2.41e-2
LAAF	7.30e-3	9.44e-4	7.23e-4	7.35e-2
PirateNet	1.98e-3	9.73e-3	4.54e-3	1.39e-2
ABU-PINN			2.98e-3	
Mask-PINN	<u>6.93e-4</u>	<u>5.26e-4</u>	<u>4.79e-4</u>	<u>1.66e-3</u>

Fig. 4 compares the pre-activation distributions of the vanilla and proposed methods at the end of training, using SoftPlus as the activation function. As the network goes deeper, the vanilla PINN shows pre-activation values that not only spread wider but also shift more to one side, making the distribution more unbalanced. In contrast, the proposed method more effectively regulates the pre-activation distribution, maintaining a more centered and stable

form. This suggests that during training, the vanilla method’s pre-activations tend to drift toward the linear regime of the SoftPlus activation function, which can negatively impact both the training dynamics and the model’s expressiveness. This phenomenon helps explain why our method yields significantly better performance when using SoftPlus.

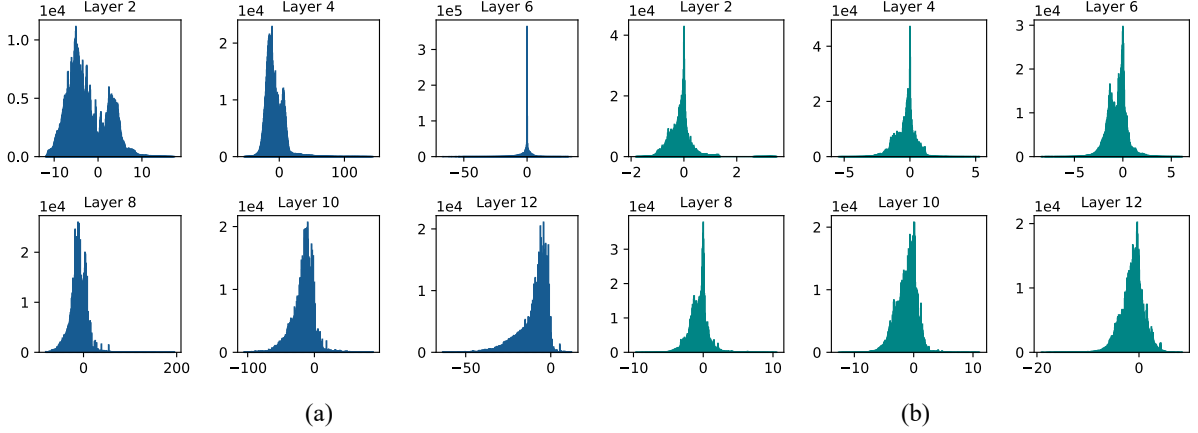


Figure 4. Convection Equation: pre-activation distributions of the vanilla and proposed methods with SoftPlus activation. (a) Vanilla method. (b) Proposed method.

4.2 1D Wave Propagation

Here we consider the 1D wave propagation equation as:

$$\frac{\partial^2 u}{\partial t^2} = c^2 \frac{\partial^2 u}{\partial x^2}, \quad (x, t) \in [0, 1] \times [0, 5], \quad (20)$$

$$u(0, t) = u(1, t) = 0, \quad t \in [0, 5], \quad (21)$$

$$u(x, 0) = \sin(\pi x), \quad x \in [0, 1], \quad (22)$$

$$\frac{\partial u}{\partial t}(x, 0) = 0, \quad (23)$$

the analytical solution for this problem is:

$$u(x, t) = \sin(\pi x) \cos(c\pi t). \quad (24)$$

Here we set $c = 1$. All the models have 7 hidden layers, each containing 256 neurons, and is trained for 20,000 iterations. For the proposed method, α is initialized with all entries set to 1.0.

Table 2: 1D Wave propagation: relative L^2 errors of different models.

Method	Tanh	GELU	SiLU	SoftPlus
Vanilla	7.33e-2	5.09e-3	8.52e-3	3.61e-2
ResNet-PINN	4.85e-2	7.52e-3	5.22e-3	7.67e-1
LAAF	1.04e-2	4.37e-3	5.73e-3	1.31e-2
PirateNet	1.59e-2	8.83e-3	9.95e-3	5.04e-2
ABU-PINN	4.82e-2			
Mask-PINN	<u>2.39e-3</u>	<u>2.90e-3</u>	<u>4.82e-3</u>	<u>6.38e-3</u>

Table 2 shows the outcomes of different models. Interestingly, while the vanilla method yielded the poorest performance with Tanh, the proposed method achieved its best result using the same activation function. Fig. 5 presents the variance changing of the proposed method and vanilla method with Tanh as activation function. It clearly shows that for vanilla method, the variance increases notably with training, suggesting severe distribution drift. The variance curves of the proposed method show relatively smaller values and stable trends after

initial iterations, indicating controlled variance growth. This reflects effective regulation of pre-activations as depth and training progress.

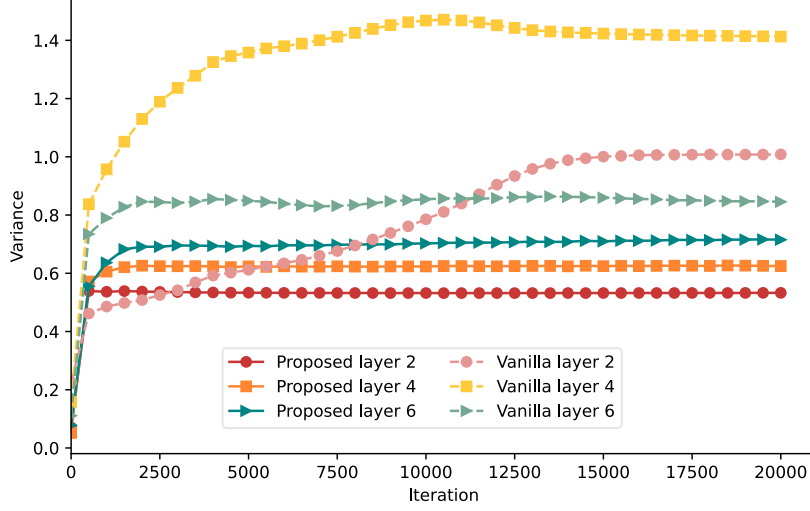


Figure 5. 1D wave propagation equation: variances of pre-activations of vanilla and proposed methods with Tanh activation.

4.3 Helmholtz equation

We consider the Helmholtz equation expressed as below:

$$\frac{\partial^2 u}{\partial x^2} + \frac{\partial^2 u}{\partial y^2} + k^2 u - q(x, y) = 0, \quad x \in [-1, 1], \quad y \in [-1, 1], \quad (25)$$

$$u(-1, y) = u(1, y) = u(x, -1) = u(x, 1) = 0, \quad (26)$$

where the source term $q(x, y)$ is in the form of:

$$\begin{aligned} q(x, y) = & -(a_1 \pi) \sin(a_1 \pi x) \sin(a_2 \pi y) \\ & -(a_2 \pi) \sin(a_1 \pi x) \sin(a_2 \pi y) \\ & + k^2 \sin(a_1 \pi x) \sin(a_2 \pi y), \end{aligned} \quad (27)$$

here we set $a_1 = 6$, $a_2 = 6$ and $k = 1$.

All models are composed of 11 hidden layers with 128 neurons each, except PirateNet, which uses 10 hidden layers. Each model is trained for 50,000 iterations.

For the proposed method, α is initialized with all entries set to 1.0 for GELU and SiLU, 5.0 for Tanh, and 2.0 for SoftPlus.

Table 3: Helmholtz equation: relative L^2 errors of different models.

Method	Tanh	GELU	SiLU	SoftPlus
Vanilla	9.37e-1	7.20e-1	1.00	1.00
ResNet-PINN	3.48e-1	8.02e-1	7.10e-1	1.00
LAAF	3.26e-2	2.26e-2	1.93e-1	5.89e-1
PirateNet	1.17	3.56e-2	2.68e-1	7.15e-1
ABU-PINN		2.83e-2		
Mask-PINN	<u>9.94e-3</u>	<u>1.52e-2</u>	<u>1.99e-2</u>	<u>1.75e-2</u>

Table 3 shows the outcomes of different models. As can be seen, the proposed method achieves the best performance across different activation functions. Notably, for activation functions SiLU and SoftPlus, other methods fail to get satisfactory results. In contrast, our

model maintains comparable accuracy across all activation functions. This highlights its robustness across different activation functions.

As the Vanilla method achieves its best performance under GELU, we present the averaged loss curves of different models using GELU as the activation function in Fig. 6. (ABU-PINN is excluded as it dynamically selects activation functions during training.) As shown in Fig. 6, the proposed method converges faster and reaches a lower final loss.

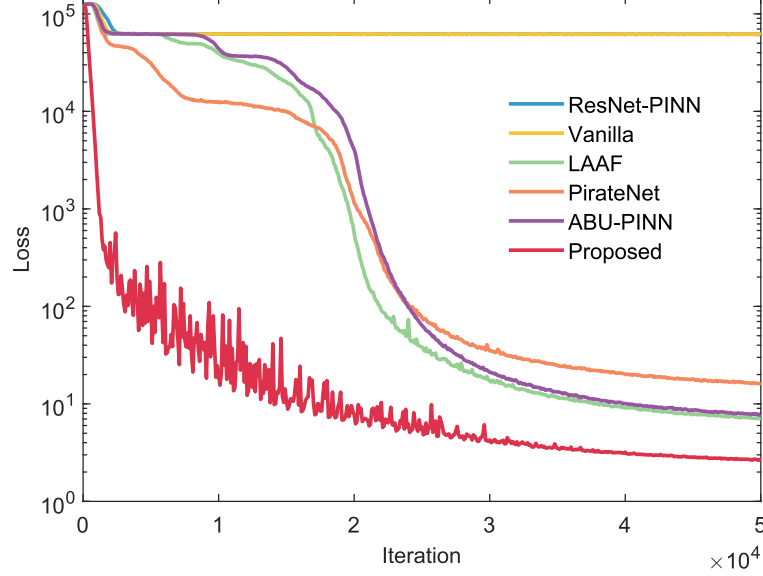


Figure 6. Helmholtz equation: averaged loss curves of different models with GELU as activation function.

Fig. 7 shows the loss landscapes of vanilla method and the proposed method with GELU as activation function. We visualize the loss landscape by perturbing the trained model along the first two leading eigenvectors of the Hessian and evaluating the loss at each perturbed point. It's evident that proposed method gets smoother loss landscape. For vanilla method, the surface is highly non-smooth, with many sharp spikes and irregular fluctuations. The irregular and rugged nature of the loss landscape indicates a tendency for the optimizer to become trapped in local minima with high loss value, which is consistent with the loss curve shown in Figure 6.

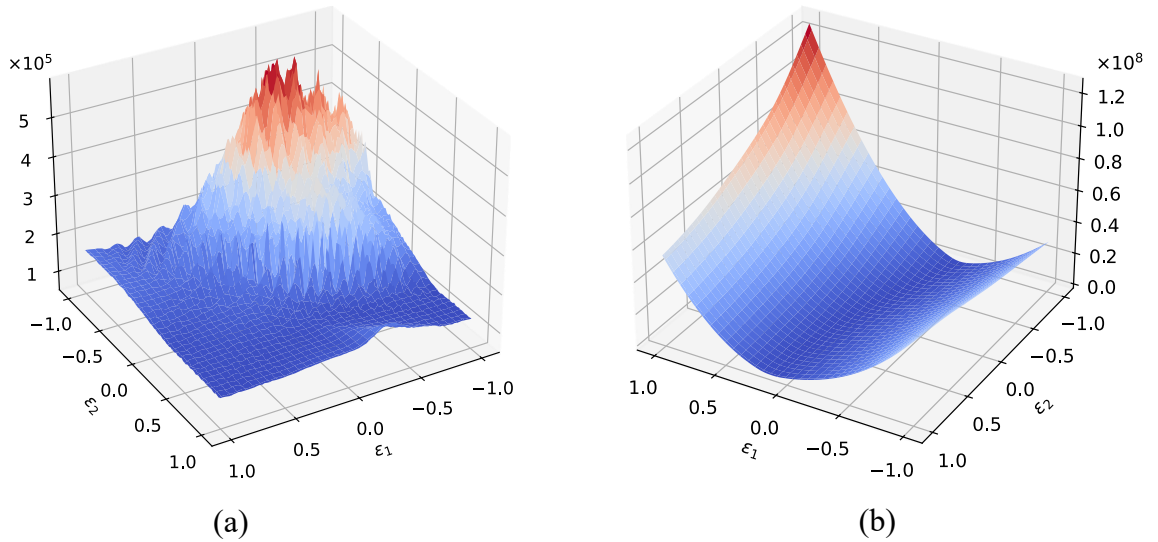


Figure 7. Helmholtz equation: loss landscapes of vanilla method and the proposed method with GELU as activation function. (a) Vanilla method. (b) Proposed method.

4.4 Wider Structure

Although it is commonly known that deeper and wider neural networks can improve approximation capability, for PINNs the situation is quite different. Theoretical analysis and empirical experiments have proved that the PINNs will degrade when the NNs become wider or deeper [8]. While some solutions have been proposed to address the degradation problem in deep PINN architectures [8], [10], [23], the challenge of effectively utilizing wider architectures remains largely unexplored. Here we show that with the proposed method, PINNs can effectively utilize wider structure.

With the Convection equation mentioned above, we conduct experiments on neural networks with different widths across different activation functions. For all the neural networks, we fix the depth as 3 hidden layers. Other settings are aligned with section 4.1. All the results are averaged from 5 independent trials. As shown in Fig. 8. Vanilla PINNs suffer from degradation issue as the width of the neural network increases. For the proposed method, a consistent improvement is witnessed as the neural network becomes wider. This indicates that with the proposed method can effectively mitigate the degradation problem seen in vanilla PINNs. Consequently, the proposed method allows PINNs to utilize wider structures, enhancing their robustness and accuracy.

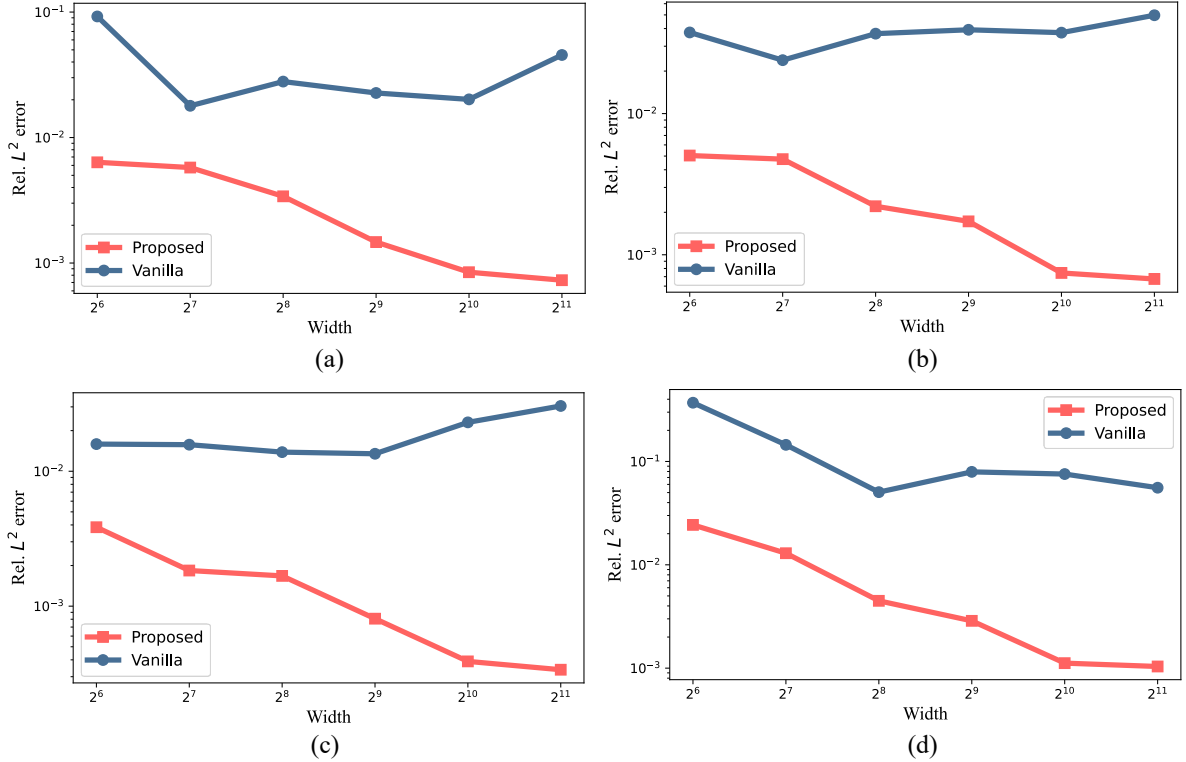


Figure 8. Relative L^2 errors of vanilla PINNs and the proposed method across various network width. (a) GELU activation function. (b) SiLU activation function. (c) Tanh activation function. (d) SoftPlus activation function.

To further explore the underlying reasons behind this improvement, we present the pre-activation distributions of the vanilla and proposed methods in Fig. 9. It clearly shows that with the width increasing, the pre-activation distribution of vanilla PINNs tends to drift away from the center. Also note that for the GELU, SiLU, and SoftPlus activation functions, the pre-activation distributions in the vanilla method exhibit a clear tendency to drift toward the negative range. This suggests that neurons may become inactive or saturated due to these activation functions' asymmetric activation properties, which severely limit the network's

expressive power. The proposed method can effectively retain the balanced distribution shape, with a narrower variance.

The results presented above highlight that the feature distribution instability and neuron saturation issues of wider neural networks lead to the degradation of PINNs. Our approach directly mitigates these issues by maintaining stable pre-activation distributions, allowing wider architectures to maintain their representational capability and achieve better accuracy.

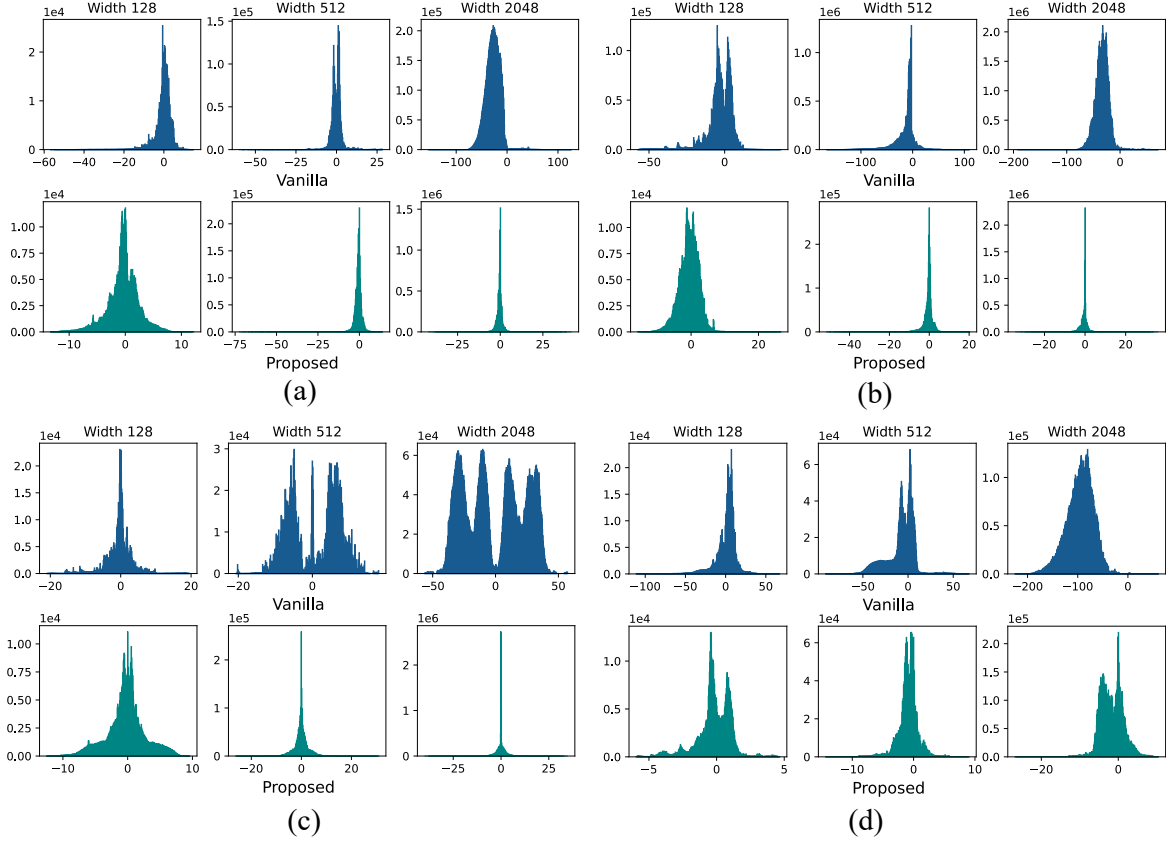


Figure 9. The pre-activation distributions of the 3rd hidden layer at the end of the training. (a) GELU activation function. (b) SiLU activation function. (c) Tanh activation function. (d) SoftPlus activation function.

5 Conclusion

In this paper, we proposed Mask-PINNs, a novel architecture designed to alleviate the issue of internal covariate shift in Physics-Informed Neural Networks without destroying the given physical laws. By introducing a learnable mask function, Mask-PINNs effectively mitigate internal covariate shift, achieving improved stability, accuracy, and robustness across a variety of PDE benchmarks and activation functions. Our experiments demonstrate that Mask-PINNs not only outperform existing methods across different settings but also enable the effective use of wider network architectures. By stabilizing feature distributions, Mask-PINNs provide a simple yet powerful tool for enhancing the representational capability of PINNs. The introduction of Mask-PINNs represents a significant advancement towards stable and scalable neural network architectures for solving PDEs, opening several exciting avenues for future exploration in physics-informed deep learning.

While our results are promising, further investigations are warranted. We found that the initial value of the scaler α plays a critical role in training dynamics. Building on these findings, future research should explore a more systematic study of how to better initialize the scaler depending on the task and network configuration.

References

- [1] M. Raissi, P. Perdikaris, and G. E. Karniadakis, "Physics-informed neural networks: A deep learning framework for solving forward and inverse problems involving nonlinear partial differential equations," *Journal of Computational physics*, vol. 378, pp. 686-707, 2019.
- [2] X. Jia *et al.*, "Physics guided RNNs for modeling dynamical systems: A case study in simulating lake temperature profiles," in *Proceedings of the 2019 SIAM international conference on data mining*, 2019: SIAM, pp. 558-566.
- [3] M. Raissi, A. Yazdani, and G. E. Karniadakis, "Hidden fluid mechanics: Learning velocity and pressure fields from flow visualizations," *Science*, vol. 367, no. 6481, pp. 1026-1030, 2020.
- [4] S. Cai *et al.*, "Artificial intelligence velocimetry and microaneurysm-on-a-chip for three-dimensional analysis of blood flow in physiology and disease," *Proceedings of the National Academy of Sciences*, vol. 118, no. 13, p. e2100697118, 2021.
- [5] J. Zhang and X. Zhao, "Three-dimensional spatiotemporal wind field reconstruction based on physics-informed deep learning," *Applied Energy*, vol. 300, p. 117390, 2021.
- [6] H. Wang, L. Lu, and G. Huang, "Learning Specialized Activation Functions for Physics-Informed Neural Networks," *Communications in Computational Physics*, vol. 34, no. 4, pp. 869-906, 2023.
- [7] J. Zhang and C. Ding, "Simple yet effective adaptive activation functions for physics-informed neural networks," *Computer Physics Communications*, vol. 307, p. 109428, 2025.
- [8] S. Wang, B. Li, Y. Chen, and P. Perdikaris, "PirateNets: Physics-informed Deep Learning with Residual Adaptive Networks," *arXiv preprint arXiv:2402.00326*, 2024.
- [9] M. Cooley, R. M. Kirby, S. Zhe, and V. Shankar, "HyResPINNs: Adaptive Hybrid Residual Networks for Learning Optimal Combinations of Neural and RBF Components for Physics-Informed Modeling," *arXiv preprint arXiv:2410.03573*, 2024.
- [10] F. Jiang, X. Hou, and M. Xia, "Element-wise multiplication based deeper physics-informed neural networks," *arXiv preprint arXiv:2406.04170*, 2024.
- [11] S. Wang, A. K. Bhartari, B. Li, and P. Perdikaris, "Gradient Alignment in Physics-informed Neural Networks: A Second-Order Optimization Perspective," *arXiv preprint arXiv:2502.00604*, 2025.
- [12] Q. Liu, M. Chu, and N. Thuerey, "Config: Towards conflict-free training of physics informed neural networks," *arXiv preprint arXiv:2408.11104*, 2024.
- [13] V. Sitzmann, J. Martel, A. Bergman, D. Lindell, and G. Wetzstein, "Implicit neural representations with periodic activation functions," *Advances in neural information processing systems*, vol. 33, pp. 7462-7473, 2020.
- [14] H. woo Lee, H. Choi, and H. Kim, "Robust Weight Initialization for Tanh Neural Networks with Fixed Point Analysis," in *The Thirteenth International Conference on Learning Representations*.
- [15] S. Ioffe and C. Szegedy, "Batch normalization: accelerating deep network training by reducing internal covariate shift," presented at the Proceedings of the 32nd International Conference on International Conference on Machine Learning - Volume 37, Lille, France, 2015.
- [16] C. Nwankpa, W. Ijomah, A. Gachagan, and S. Marshall, "Activation functions: Comparison of trends in practice and research for deep learning," *arXiv preprint arXiv:1811.03378*, 2018.

- [17] S. R. Dubey, S. K. Singh, and B. B. Chaudhuri, "Activation functions in deep learning: A comprehensive survey and benchmark," *Neurocomputing*, vol. 503, pp. 92-108, 2022.
- [18] C. Tsvetkov, G. Malhotra, B. D. Evans, and J. S. Bowers, "The role of capacity constraints in Convolutional Neural Networks for learning random versus natural data," *Neural Networks*, vol. 161, pp. 515-524, 2023.
- [19] X. Glorot and Y. Bengio, "Understanding the difficulty of training deep feedforward neural networks," in *Proceedings of the thirteenth international conference on artificial intelligence and statistics*, 2010: JMLR Workshop and Conference Proceedings, pp. 249-256.
- [20] M. Lee, "Mathematical analysis and performance evaluation of the gelu activation function in deep learning," *Journal of Mathematics*, vol. 2023, no. 1, p. 4229924, 2023.
- [21] J. L. Ba, "Layer normalization," *arXiv preprint arXiv:1607.06450*, 2016.
- [22] T. Salimans and D. P. Kingma, "Weight normalization: A simple reparameterization to accelerate training of deep neural networks," *Advances in neural information processing systems*, vol. 29, 2016.
- [23] A. Aygun, R. Maulik, and A. Karakus, "Physics-informed neural networks for mesh deformation with exact boundary enforcement," *Engineering Applications of Artificial Intelligence*, vol. 125, p. 106660, 2023.